Available online at www.sciencedirect.com
ScienceDirect
Surface & Coatings Technology 202 (2008) 4728–4733
SURFACE & COATINGS TECHNOLOGY
www.elsevier.com/locate/surfcoat

The tensile properties of titanium processed by surface mechanical attrition treatment

Ming Wen [a,b], Gang Liu [a,*], Jian-feng Gu [c], Wei-ming Guan [b], Jian Lu [d,*]

[a] Shenyang National Laboratory for Materials Science, Institute of Metals Research, Chinese Academy of Sciences, Shenyang, 110016, People's Republic of China
[b] Kunming Institute of Precious Metals, Kunming, 650106, People's Republic of China
[c] School of Materials Science and Engineering, Shanghai Jiao Tong University, Shanghai, 200240, People's Republic of China
[d] Mechanical Engineering Department, The Hong Kong Polytechnic University, Hong Kong, People's Republic of China

Received 17 December 2007; accepted in revised form 4 April 2008
Available online 16 April 2008

Abstract

In this work, the tensile properties of nanocrystalline Ti and bulk Ti processed by surface mechanical attrition treatment (SMAT) have been studied. The nanocrystalline Ti shows high strength which can be comparable to that of Ti–6Al–4V together with depressed plasticity. On the contrary, the strength of bulk Ti after SMAT is obviously improved with acceptable ductility and this new material has a potential biomedical application.

PACS: 61.46.Hk; 62.20Fe
Keywords: SMAT; Titanium; Nanocrystalline materials; Tensile properties

1. Introduction

The use of titanium and its alloys in biomedical field have become a well established area due to their lower modulus, superior biocompatibility and enhanced corrosion resistance as compared with the more conventional stainless steels and cobalt-based alloys [1–3]. Until now, the most important implant materials are commercial pure (CP) Ti and Ti–6Al–4V. Ti–6Al–4V alloy, being developed for aerospace industry firstly, has been considered not appropriate in human body for Al and V are toxic and may potentially cause a series of ailments including cancer. CP Ti is chemically inert and biologically more compatible than Ti–6Al–4V, but coarse-grained (CG) Ti has low wear and abrasion resistance because of its low hardness [3]. Nanocrystalline (nc) and ultrafine-grained (UFG) materials have exhibited many novel properties such as high strength and hardness, as well as excellent tribological properties relative to their CG counterparts [4–6]. Due to the various limitations of present methods, preparation of ideal bulk nc sample (free of contamination and porosity, bulk in size, uniform and small grain size) is still a challenge to materials scientists [7]. The typical method to UFG Ti is equal-channel angular pressing (ECAP), and the processing temperature is usually 400–450 °C to enhance the workability [8]. In fact, recovery, a thermally activated process, increases its rate exponentially with temperature resulting in larger grain size (usually 200–300 nm for ECAP) and lower dislocation density in Ti. And additional steps such as cold rolling, high pressure torsion (HPT), or cold extrusion should be conducted following ECAP for further refining the grain size [9–12].

In fact, most failures of materials occurring on surfaces (fatigue fracture, fretting fatigue, wear and corrosion etc.) are very sensitive to the surface structure and properties, and the surface-optimization may effectively enhance the overall properties of materials. As concerned with the superior properties of nc materials, Lu et al. put forward that the global properties and behaviors will be greatly improved if a nc layer could be generated on a material surface [13,14]. Based on the

* Corresponding authors. Liu is to be contacted at Shenyang National Laboratory for Materials Science, Institute of Metals Research, Chinese Academy of Sciences, Shenyang, 110016, People's Republic of China. Lu, Mechanical Engineering Department, The Hong Kong Polytechnic University, Hong Kong, People's Republic of China. Tel.: +86 852 27666665; fax: +86 852 2365 4703.
E-mail addresses: gliu@imr.ac.cn (G. Liu), mmmelu@inet.polyu.edu.hk (J. Lu).

0257-8972/$ - see front matter © 2008 Elsevier B.V. All rights reserved.
doi:10.1016/j.surfcoat.2008.04.054

principle of surface nanocrystallization, surface mechanical attrition treatment (SMAT), an effective way to realize surface self-nanocrystallization on metallic materials without changing the chemical compositions, was proposed and has been realized in many metals and alloys such as Fe, AISI 304 stainless steel, Al-alloy, Cu, and Mg-alloy, et al. [7,15–18]. The usual SMAT process can be described as follows: Spherical steel balls are placed in the bottom and the sample to be treated is fixed in the top of a chamber which is vibrated by a vibration generator. When the balls are resonated, the sample surface is impacted by a large number of flying balls with random flying directions over a short period of time. In a word, the key point of SMAT is to introduce a large amount of defects and/or interfaces into the surface layer of treated materials by repeated multidirectional impacts at high strain rate over a short period of time, so the grain size of entire sample surface is transformed from CG into nanometer scale progressively. [14]. As compared with ECAP, SMAT could be conducted at room temperature and the temperature rise during process is very limited which will be much helpful for the grain refinement. In this work, the tensile properties of Ti processed by SMAT was studied which is important both from academic and applied points of view.

2. Experimental

The material used in this study was a CP Ti plate with the chemical composition (wt.%): 0.10 Fe, 0.01 Si, 0.16 O, 0.014 N, 0.004 H, 0.022 C, 0.23 Al and balance Ti. The plate was annealed in argon atmosphere at 740 °C for 2 h, and then air-cooled, resulting in equiaxed grains averaging 30 μm in size. The SMAT set-up had been described in details elsewhere [13,14]. In this study, the vibration frequency of the system was 50 Hz, stainless steel balls with the diameter of 8 mm were used and the samples were treated in vacuum for 60 min at room temperature (RT). A Rigaku D/max-2400 X-ray diffractometer (12 kW) with Cu K_α radiation was used to determine the phase constitution and the mean grain size. The grain size and micro-strain were calculated from line broadening of Bragg diffraction peaks by using Scherrer and Wilson method [19]. Transmission electron microscopy (TEM) images and the corresponding selected area electron diffraction (SAED) were obtained by using a JEOL 2010 TEM with an accelerating voltage of 200 kV. A 300 kV Tecnai G^2 F30 TEM instrument, which was equipped with a high-angle annular dark-field (HAADF) detector in the STEM system and a post-column Gatan imaging filter system, was used for high-resolution imaging.

The tensile specimens of nc layers were prepared as follows. The top surface was removed about 6 μm thick to get rid of the surface roughness effect firstly. Secondly, dogbone-shaped tensile specimens were cut from the top surface layer (about 500 μm thick) by using electro-discharging. Then they were carefully mechanical polished from the untreated side until the thickness was about 20 μm. The final tensile specimen geometry has a gauge length of 4 mm, a cross-sectional area of 2 mm × 0.02 mm, and the radius between the gauge length and the grip ends of 2.5 mm. Three repeated tensile tests were performed. The dimensions of the tensile specimens were firstly measured by Leica MPS 30 optical microscopy, and finally checked by the Supra 35 LEΦ field emission scanning electron microscopy (FSEM). Tensile tests were carried out on a Tytron 250 Micro-force Testing System at a strain rate $6 \times 10^{-3}\ s^{-1}$ at RT. The tensile specimens of bulk tensile samples were prepared as follows. A Ti plate with thickness of 1 mm was SMATed from both sides (each side for 60 min, respectively). After cutting and mechanical polishing, the final tensile specimen geometry has a gauge length of 5 mm, a cross-sectional area of 2 mm × 1 mm, and the radius between the gauge length and the grip ends of 2.5 mm. Tensile tests were carried out on an Instron micro tester 5848 at a strain rate $6 \times 10^{-3}\ s^{-1}$ at RT and four repeated tensile tests were performed. For comparison, four CG tensile specimens with the same geometry as bulk SMAT Ti were also tested under the same conditions. The fracture surface observations were conducted by the Supra 35 LEΦ field emission scanning electron microscopy (FSEM) and FEI quanta 600 scanning electron microscopy (SEM).

3. Results and discussion

Fig. 1 shows XRD results of the surface layer in CG and SMAT Ti. Evident Bragg-diffractional peak broadening exists in SMAT Ti, which is caused by the grain refinement and an increase in the atomic-level micro-strain. The average grain size calculated by Scherrer and Wilson method was about 43 nm, and the micro-strain was about 0.18%.

Fig. 2 shows the TEM images and grain size distribution of SMAT Ti at top surface. Some of the grains are irregular and some grain boundaries are not well defined suggesting the presence of high internal stress and non-equilibrium grain boundaries due to the high density of dislocations. The grain size varies from 10 to 130 nm with an average grain size about 30 nm measured from a number of TEM images. The mean grain size is smaller than that calculated by XRD (43 nm), since XRD analysis averages the structure information of a much thicker layer than TEM. Previous studies had showed: (1) the

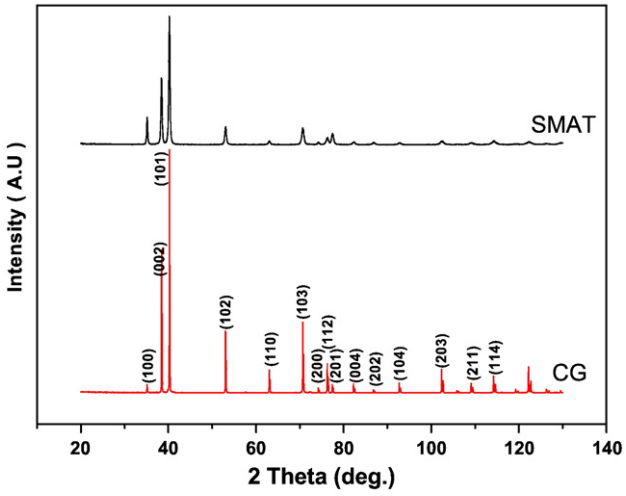

Fig. 1. XRD results of the surface layer in coarse-grained and SMAT Ti.

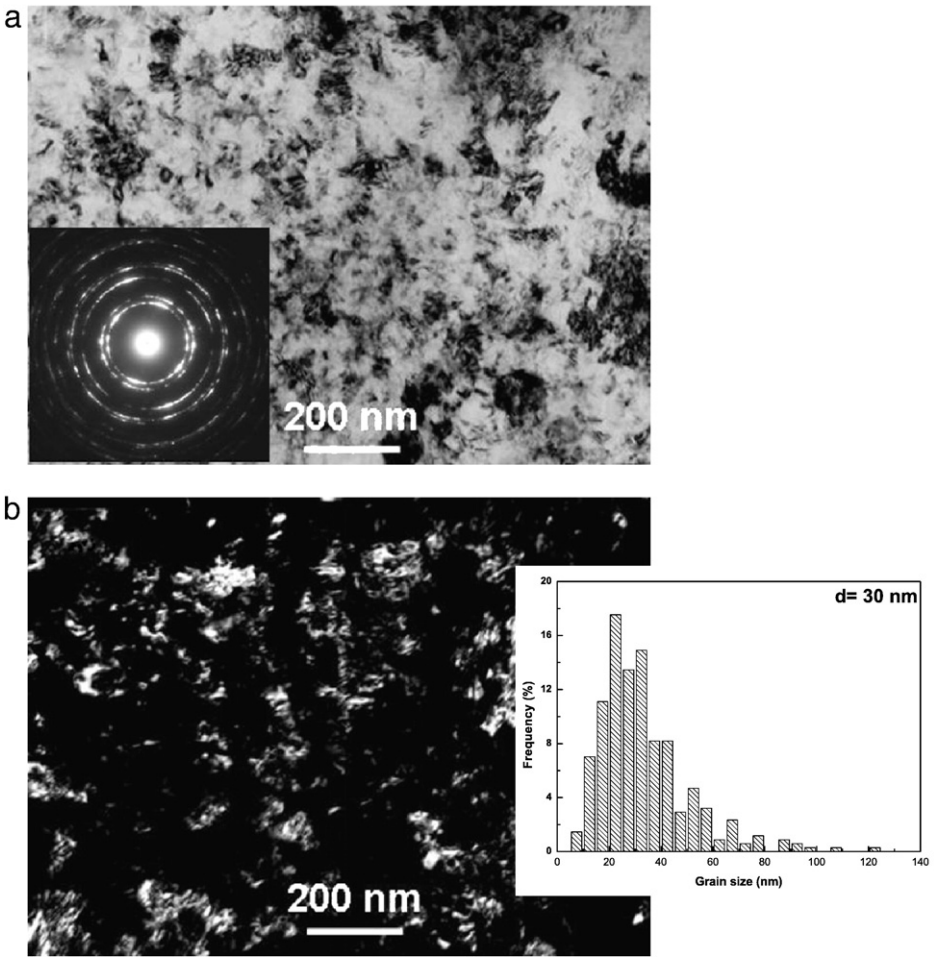

Fig. 2. (a): bright field image; (b): dark-field TEM image and grain size distribution of SMAT Ti at top surface.

thickness of the total deformation layers was about 150–200 μm; and (2) the mean grain size at 15 μm below top surface was 100 nm, below which the microstructure was characterized by UFG Ti, lamellar-like subgrain, dislocation tangles, and deformation twins, respectively [20,21].

Tensile engineering stress–strain curves of nc Ti, bulk SMAT Ti, and CG counterpart are shown in Fig. 3. In nc Ti, the yield strength (0.2% offset) and the ultimate tensile strength (UTS) are 920±40 MPa and 970±30 MPa, respectively. The values are much higher than those of CG Ti, and even can be comparable to those of Ti–6Al–4V (yield strength=902 MPa, UTS=975 MPa) [22]. In the same time, nc Ti shows a depressed ductility with a total elongation no more than 2.0%. The results of high strength and low ductility have also been found previously for nc Cu and nc 316 L austenitic stainless steel processed by SMAT [23,24]. On the contrary, the yield strength and UTS of bulk SMAT Ti increase by about 100 MPa respectively as compared with CG sample together with acceptable ductility (uniform elongation of bulk SMAT Ti is about 59% of CG sample).

Fig. 4 is the SEM images of fracture surfaces of the nc Ti (a), bulk SMAT Ti (b), and CG Ti (c). All of them show clear ductile features. The mean dimple size in nc Ti is only about 720 nm, and it is also clear that there exist some large dimples of 1–2 μm which may be caused by coalescence of some small dimples during straining. As a contrast, the mean dimple size of CG Ti is about 16 μm. The very fine dimples cause smaller local stress concentration in unfractured ligaments near the dimple edge than large dimples in CG Ti, which makes nc Ti more resistant

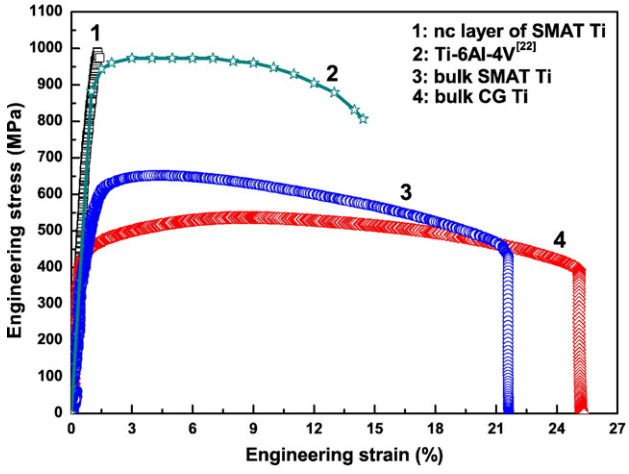

Fig. 3. Tensile engineering stress–strain curves for nc Ti by SMAT, bulk SMAT Ti, and CG counterpart.

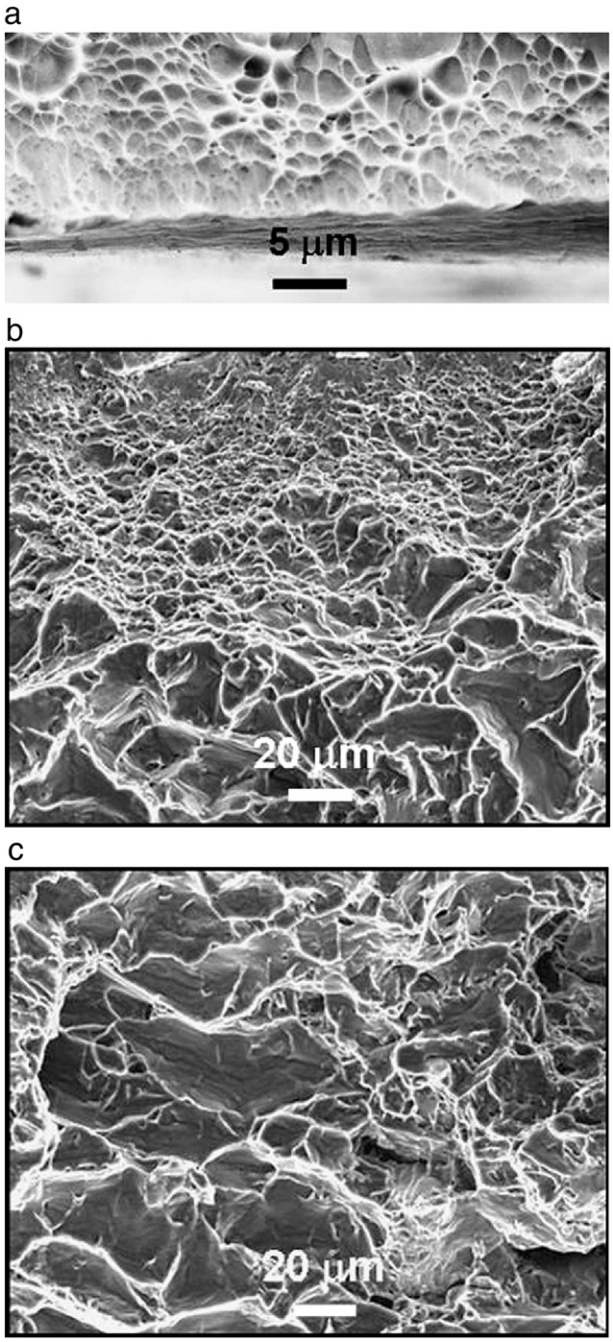

Fig. 4. SEM images of fracture surfaces of the nc Ti (a), bulk SMAT Ti (b), and CG Ti (c).

to fracture [9]. Accordingly, bulk SMAT Ti shows a gradient structured dimple size which varies from 720 nm to 16 μm from treated surface to strain-free matrix (Fig. 4c).

The high strength of nc Ti could be attributed to the grain size, dislocations, and residual compressive stresses. During the SMAT procedure, due to the rapid decrease of strain and strain rate with distance from treated surface, residual compressive stresses were generated from the nonhomogeneous plastic deformation between surface and subsurface. The macroscopic residual stresses were greatly reduced during sample preparation, and thus contribute very little to the high strength in nc Ti [24]. So fine grain size and dislocations are the main reasons for the high strength of nc Ti. In fact, the strength of conventional polycrystals dependences on mean grain size can be described by well-known Hall–Petch relations:

$$\sigma_y = \sigma_0 + Kd^{-\frac{1}{2}}. \quad (1)$$

Where σ_y is the yield strength; d is the average grain size; σ_0 and k are material constants. As for Ti, $\sigma_0 = 134.2$ MPa and $k = 0.671$ MPa·m$^{-1/2}$ [9,25]. By using the grain size of 100 nm at about 15 μm below top surface, the yield strength calculated was much higher than the experimental data. Zhu et al. [9] also found the same results in UFG Ti processed by two-step SPD (ECAP followed by cold rolling), suggesting Hall–Petch relations maybe not appropriate in nc/UFG Ti produced by SPD. The grain size of present nc Ti is much smaller than those by other SPD methods such as ECAP, HPT and repeat cold-rolling [8–12, 26], which can be attributed to the temperature and strain rate effects. Semiatin et al. [27] conducted ECAP of Ti from 25 to 325 °C with different strain rates, and they found Ti underwent segmented failure under all conditions except at low strain rates and high temperature. Raab et al. [28] studied the temperature and the hydrostatic pressure during ECAP and concluded that the decrease of ECAP temperature and the increase of hydrostatic pressure in deformation zone contribute to the formation of finer grains. As we mentioned before, ECAP is usually carried out at 400–450 °C to ensure sufficient ductility, but in the same time, recovery, a thermal activated process, will increase exponentially with temperature resulting in large grain size and low dislocations densities. As concerned with SMAT method, the materials can be processed at RT, and the temperature rising on sample surface is very limited as compared with ECAP. For example, the temperature rising was about 50–100 °C in a Fe sample surface during repeat impacts [14]. Recovery process is also time-dependent, and the increasing of strain rate during plastic deformation may result in higher dislocation density and finer grain size. During SMAT, the strain rate on material top surface (10^2–10^3) is much higher than other SPD method such as ECAP. So the low deformation temperature and high strain rates suppress dynamic recovery in SMAT and result in higher dislocation density facilitating the grain refinement of Ti to about 30 nm on top surface. The nc Ti on top surface was irregular shape, which is different from the equiaxed grains in Fe, Cu, and Mg alloy, and high-resolution TEM (HRTEM) investigations were further conducted to investigate the dislocation distribution. Fig. 5a shows a HRTEM image of a nc Ti on top surface, and a square of 7×7 nm^2 was selected for fourier transform. As shown in Fig. 5b, there are six dislocations within this regime suggesting nc Ti is in a non-equilibrium state. It is generally agreed that the subgrain size levels off, and grain subdivision cannot continue indefinitely at very large plastic deformation. But plastic deformation usually increases the misorientations across fragment boundaries even when the average fragment sizes no longer decrease [29]. The increasing of misorientations between neighboring grains can be realized by accumulation and annihilation of more dislocations in grain boundaries, or alternatively, by rotation of grains (or grain

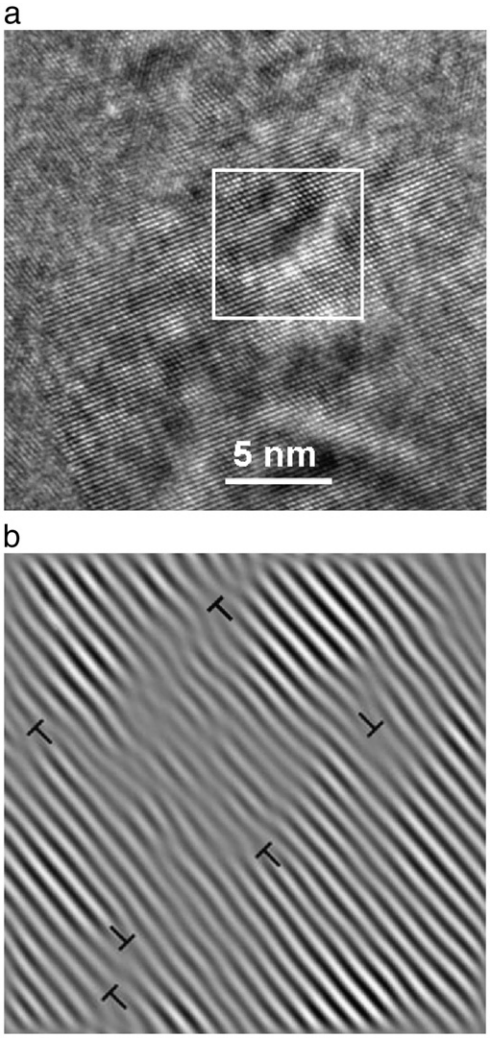

Fig. 5. (a): the HRTEM image of SMAT Ti at top surface; (b): the corresponding fourier transform of square in (a).

boundary sliding) with respect to each other under certain strains [7].

The failure of nc Ti happened shortly after yield with little strain hardening (Fig. 3). According to the well-known Consideré criterion for necking,

$$\left(\frac{\partial \sigma}{\partial \varepsilon}\right)_{\dot{\varepsilon}} \leq \sigma. \tag{2}$$

Where σ and ε are true stress and true strain, respectively. Considering the high strength (σ) and low strain hardening rate $\left(\frac{\partial \sigma}{\partial \varepsilon}\right)$ of nc materials, it is very easy to satisfy the necking condition and inhomogeneous deformation happens even at low strain. The strain hardening exponent (n) for materials can be calculated by fitting the equation:

$$\sigma = K'\varepsilon^n. \tag{3}$$

Where σ and ε are true stress and true strain, respectively; k' is constants. The n value for nc Ti, bulk SMAT Ti, and CG Ti is 0.016, 0.060, and 0.090, respectively. The UFG/nc Ti has shown limited ductility at room temperature [9,30]. Due to the small grain size of nc Ti, the grain boundaries can act as both dislocation sources and sinks, with dislocations bowing out of one segment of a grain boundary and disappearing in another segment across the grain during deformation. In severe deformed microstructures, the dissociation of trapped lattice dislocations is more prevalent at non-equilibrium grain boundaries, which induces recovery [31]. Due to the non-equilibrium state of nc Ti revealed by TEM observations (Figs. 2 and 5), the dynamic recovery would take place easily and play an important role in the absence of the strain hardening. In other words, the dislocations generation and annihilation are approaching dynamic balance with no significant change during further plastic deformation. So the strain hardening of nc Ti by SMAT remains very limited and far less than that of CG counterparts. Meanwhile, the tendency for plastic instability is enhanced and the necking instability begins very quickly during tension. This vulnerability to localized deformation/failure modes is believed to be at least partly responsible for the limited tensile uniform deformation and elongation to failure observed for vast majority of nc/UFG materials that are ductile at CG regime [32]. Bulk SMAT Ti shows improved strength while retains sufficient strain hardening capability as compared with nc Ti. The grain size of bulk SMAT Ti gradually varies from nc to micrometer regime from treated surface to matrix, and nc grain provides high strength while CG Ti supplies the strain hardening capability which prevents localized deformation and premature fracture. A similar phenomenon was observed in a 316 L stainless steel sample in which both yield strength and UTS are enhanced [33]. Analysis of the fracture mechanism revealed that the nanostructured surface layers on both sides of SMAT 316 L stainless steel sample blocked the slip bands developed in CG matrix. So crack nucleation will occur in the subsurface layers but not in sample surface due to the much enhanced nc layers, and the dislocation jam-packing leads to the material hardening. It is should be noted that the strength of bulk SMAT Ti is higher than that calculated by the widely used rule of mixtures, suggesting a compressive residual stress, which can effectively inhibit the initiation and the propagation of microcracks in the surface, also contributes to the strength.

4. Conclusion

Nanocrystalline Ti with high strength could be made by SMAT. The low deformation temperature and high strain rates suppress dynamic recovery in SMAT, and thus facilitate the grain refinement of Ti (~30 nm). In the same time, the depressed strain hardening of nc Ti can be attributed to the small grain size with nearly saturated dislocation density. On the contrary, bulk SMAT Ti shows good mechanical properties which combine the strengthening from nc Ti along with the strain hardening provided by dislocation activity in CG Ti.

Acknowledgements

This work was supported by the NSFC (Grant No. 50431010), MOST of China (Grant No.2005CB623604) and the Hong Kong Polytechnic University (Grant No. BB90).

References

[1] T. Kokubo, H.M. Kim, M. Kawashita, T. Nakamura, J. Mater. Sci. Mater. Med. 15 (2004) 99.
[2] M. Long, H.J. Rack, Biomaterials 19 (1998) 1621.
[3] X.Y. Liu, P.K. Chu, C.X. Ding, Mater. Sci. Eng. R 47 (2004) 49.
[4] H. Gleiter, Acta Mater. 48 (2000) 1.
[5] K.S. Kumar, H. Van Swygenhoven, S. Suresh, Acta Mater. 51 (2003) 5743.
[6] M.A. Meyers, A. Mishra, D.J. Benson, Prog. Mater. Sci., 51 (2006) 427.
[7] N.R. Tao, Z.B. Wang, W.P. Tong, M.L. Sui, J. Lu, K. Lu, Acta Mater. 50 (2002) 4603.
[8] V.V. Stolyarov, Y.T. Zhu, I.V. Alexandrov, T.C. Lowe, R.Z. Valiev, Mater. Sci. Eng. A 299 (2001) 59.
[9] Y.T. Zhu, J.Y. Huang, J. Gubicza, T. Ungár, Y.M. Wang, E. Ma, R.Z. Valiev, J. Mater. Res. 18 (2003) 1908.
[10] V.V. Stolyarov, Y.T. Zhu, I.V. Alexandrov, T.C. Lowe, R.Z. Valiev, Mater. Sci. Eng. A 343 (2003) 43.
[11] V.V. Stolyarov, Y.T. Zhu, T.C. Lowe, R.Z. Valiev, Mater. Sci. Eng. A 303 (2001) 82.
[12] V.V. Stolyarov, Y.T. Zhu, T.C. Lowe, R.K. Isamgaliev, R.Z. Valiev, Nanostruct. Mater. 11 (1999) 947.
[13] K. Lu, J. Lu, J. Mater. Sci. Tech. 15 (1999) 193.
[14] K. Lu, J. Lu, Mater. Sci. Eng. A 375–377 (2004) 38.
[15] X. Wu, N. Tao, Y. Hong, B. Xu, J. Lu, K. Lu, Acta Mater. 50 (2002) 2075.
[16] H.W. Zhang, Z.K. Hei, G. Liu, J. Lu, K. Lu, Acta Mater. 51 (2003) 1871.
[17] K. Wang, N.R. Tao, G. Liu, J. Lu, K. Lu, Acta Mater. 54 (2006) 5281.
[18] H.Q. Sun, Y.N. Shi, M.X. Zhang, K. Lu, Acta Mater. 55 (2007) 975.
[19] H.P. Klug, L.E. Alexander, X-Ray Diffraction Procedures for Polycrystalline and Amorphous Materials, Wiley, New York, 1974, p. 661.
[20] M. Wen, J.F. Gu, G. Liu, Z.B. Wang, J. Lu, Surf. Coat. Technol. 201 (2007) 6285.
[21] M. Wen, J.F. Gu, G. Liu, Z.B. Wang, J. Lu, Appl. Surf. Sci. 254 (2008) 2905.
[22] H. Choe, S.M. Abkowitz, S. Abkowitz, D.C. Dunand, Mater. Sci. Eng. A 396 (2005) 99.
[23] X.H. Chen, J. Lu, L. Lu, K. Lu, Scripta Mater. 52 (2005) 1039.
[24] Y.M. Wang, K. Wang, D. Pan, K. Lu, K.J. Hemker, E. Ma, Scripta Mater. 48 (2003) 1581.
[25] A. A Salem, S.R. Kalidindi, R.D. Doherty, Scripta Mater. 46 (2002) 419.
[26] G.P. Dinda, H. Rosner, G. Wilde, Scripta Mater. 52 (2005) 577.
[27] S.L. Semiatin, V.M. Segal, R.E. Goforth, N.D. Fery, D.P. Delo, Metall. Mater. Trans. A 30 (1999) 1425.
[28] G.I. Raab, E.P. Soshnikova, R.Z. Valiev, Mater. Sci. Eng. A 387–389 (2004) 674.
[29] R.Z. Valiev, K.K. Islangaliev, I.V. Alexandrov, Prog. Mater. Sci. 45 (2000) 103.
[30] D. Jia, Y.M. Wang, K.T. Ramesh, E. Ma, Y.T. Zhu, R.Z. Valiev, Appl. Phys. Lett. 79 (2001) 611.
[31] Y.G. Ko, D.H. Shin, K.T. Park, C.S. Lee, Scripta Mater. 54 (2006) 1785.
[32] C.C. Koch, D.G. Morris, K. Lu, A. Inoue, MRS Bull. 24 (1999) 54.
[33] Y.M. Xing, J. Lu, unpublished data.